Excited State Property of Hardly Photodissociable Heme−CO Adduct Studied by Time-Dependent Density Functional Theory

Takehiro Ohta,[†] Biswajit Pal,[‡] and Teizo Kitagawa*

Okazaki Institute for Integrative Bioscience, National Institutes of Natural Sciences, Okazaki, Aichi 444-8787, Japan

Received: April 26, 2005; In Final Form: August 21, 2005

While most of CO-bound hemes are easily photodissociated with a quantum yield of nearly unity, we occasionally encounter a CO−heme which appears hardly photodissociable under the ordinary measurement conditions of resonance Raman spectra using CW laser excitation and a spinning cell. This study aims to understand such hemes theoretically, that is, the excited-state properties of the five-coordinate heme−CO adduct (5cH) as well as the 6c heme−CO adduct (6cH) with a weak axial ligand. Using a hybrid density functional theory, we scrutinized the properties of the ground and excited spin states of the computational models of a 5cH and a water-ligated 6cH (6cH−H_2O) and compared these properties with those of a photodissociable imidazole-ligated 6cH (6cH−Im). Jahn−Teller softening for the Fe−C−O bending potential in the a_1−e excited state was suggested. The excited-state properties of 6cH−Im and 5cH were further studied with time-dependent DFT theory. The reaction products of 6cH−Im and 5cH were assumed to be quintet and triplet states, respectively. According to the time-dependent DFT calculations, the Q excited state of 6cH−Im, which is initially a pure π−π* state, crosses the Fe−CO dissociative state ($2A'$) without large elongation of the Fe−CO bond. In contrast, the Q state of the 5cH does not cross the Fe−CO dissociative state but results in the formation of the excited spin state with a bent Fe−C−O. Consequently, photoisomerization from linear to bent Fe−C−O in the 5cH is a likely mechanism for apparent nonphotodissociation.

Introduction

Carbon monoxide (CO) adducts of most hemoproteins are photodissociated by visible laser illumination with a quantum yield of nearly unity.[1,2] Accordingly, photodissociation of CO is considered as an intrinsic property of CO−heme complexes. The photochemistry of CO-bound hemoglobin (COHb) and its model compounds has been explained, as illustrated in Scheme 1. The initial event is the vertical π−π* transition of heme to the ^{1}Q state, forming the Hb_I*···CO intermediate within 50 fs.[3−5] Because of the similarity of the excited-state lifetimes and absorption maxima between the Hb_I*···CO and unligated Hb (deoxyHb), the cleavage of the Fe−CO bond is considered to take place in this time scale, but it is also noted that further electronic process forming Hb_{II}* should be involved to break the Fe−CO bond, since the π−π* state is not dissociative regarding the Fe−CO bond. An Fe(III) charge transfer state[3] or a triplet spin state[4] may be a candidate. The available experimental data also indicate that the out-of-plane displacement of the Fe atom is almost instantaneously completed upon photodissociation.[3,6]

The excited states responsible for the photolysis of CO from the CO−heme complex were recently characterized by Head-Gordon and co-workers by means of time-dependent DFT (TD-DFT) theory.[7a,b] They calculated the vertical excitation energies for artificial structures of the Fe−CO bond elongated along the linear Fe−CO and concluded that Fe−CO repulsive states cross the energetically lowest and initially excited Q states at the Fe···CO separation of 2.0 Å with the activation barrier of 0.2 eV. This suggested that a vibrational wave packet on the excited potential surface can be beyond the energy barrier.[7a,b] A charge-transfer (CT) state from Fe to porphyrin was also suggested to play an important role in the CO photolysis,[7a,b] because, at an Fe−CO separation of 2.5 Å, the excited states have substantial iron-to-ligand charge-transfer character. This theoretical result was compatible with the experimental assignment of the first intermediate to the CT state by Franzen et al.[3] Similar TD-DFT analyses were also applied to explain a low quantum yield for the photolysis of a heme−O_2 adduct by Angelis and co-workers,[7c] revealing that Fe−O−O bending is effective in de-excitation of the Fe−O_2 dissociative state in the excited-state profile, while such a de-excitation mechanism does not occur for a heme−CO complex.

SCHEME 1: Proposed Photolysis Mechanism of CO-Bound Hemoglobin [Hb(CO)]

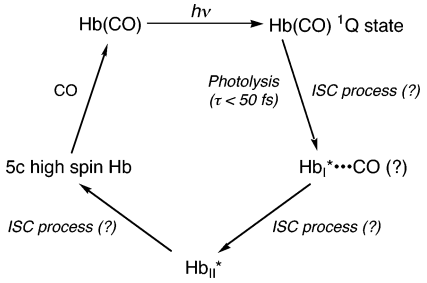

Unexpectedly, however, we have encountered in resonance Raman experiments that CO bound to the heme of soluble guanylate cyclase was not photodissociated under ordinary

* To whom correspondence should be addressed. E-mail: teizo@ims.ac.jp.
[†]Present address: Department of Chemistry, Stanford University, Stanford, CA 94305.
[‡] Present address: Centre for Cellular and Molecular Biology, Uppal Road, Hyderabad-500 007, India.

10.1021/jp052158h CCC: $30.25
Published on Web 10/14/2005

CHART 1: Model Molecules Used for DFT Calculations

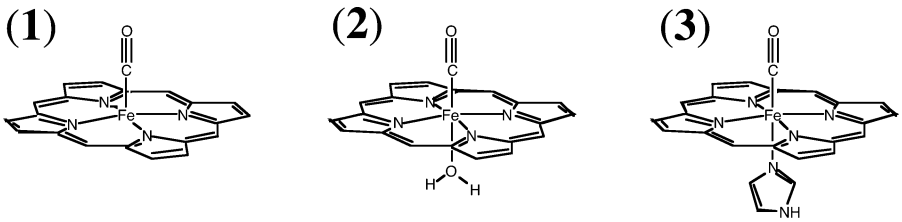

1 , **2**, and **3** represent a model of 5cH, 6cH−H_2O, and 6cH−Im, respectively. Hydrogen atoms attached to carbon atoms were omitted for clarity.

conditions, that is, CW laser excitation with a spinning cell.[8a] Our complementary experiments using iron(II)-protoporphyrin IX (hemin) in micelles of cetyl-trimethylammonium bromide (CTAB) have indicated that the five-coordinate (5c) heme−CO adduct in the CTAB micelles was also not photodissociable, while its imidazole (Im) complex is easily photodissociated in the CTAB micelles.[8b] The presence of a photoinert 5c heme−CO adduct was also suggested from a heme−copper oxidase of ba_3-cytochrome *c* oxidase from *Thermus thermophilus*, which exhibited both a photolabile six-coordinate (6c) heme−CO and a photostable 5c heme Fe−CO species.[8c] Thus, the understanding of both ground and excited electronic properties of a 5c heme−CO adduct as well as those of a 6c heme−CO adduct is crucial to elucidate the mechanism by which a heme−CO complex becomes photoinert.

This study aims to understand theoretically the properties of the 5c heme−CO adduct (5cH) as well as those of the 6c heme−CO adduct (6cH) with a weak axial ligand. Especially, we want to explain why the 5cH is not photodissociable, despite the fact that most of CO-bound hemoproteins ligated by histidine as a trans ligand are easily photodissociated. Using a hybrid density functional theory, we scrutinized the properties of the ground and excited spin states of the computational models of a 5cH and a water ligated 6cH (6cH−H_2O) and compared these properties with those of a photodissociable imidazole-ligated 6cH (6cH−Im). We characterized the relevant excited states for the photochemistry of hardly photodissociable 5cH and photodissociable 6cH−Im by using TD-DFT theory.[9]

Computational Details

The model complexes used in this study are illustrated in Chart 1; $Fe^{2+}(CO)(C_{20}N_4H_{12})^{2-}$ (**1**), $Fe^{2+}(CO)(C_{20}N_4H_{12})^{2-}(H_2O)$ (**2**), and $Fe^{2+}(CO)(C_{20}N_4H_{12})^{2-}(C_3N_2H_4)$ (**3**) are models for 5cH, 6cH−H_2O, and 6cH−Im, respectively.

All calculations were carried out on the Gaussian 98 program package[10] using the gradient-corrected B3LYP functional, which consists of the Slater exchange, the Hartree−Fock exchange, the exchange functional of Becke,[11,12] and the correlation functional of Lee, Yang, and Parr (LYP).[13] The basis set chosen for the heme−CO adducts is twofold. The first one is the 6-31G-(d) basis set for all atoms (H, C, N, O, and Fe), called the BS1 basis set, and the other, named the BS2 basis set, is the extended 6-311G+(2d) basis set[14−16] for the Fe and CO atoms, while the rest of atoms are computed with the 6-31G(d) basis set. The combination of the B3LYP functional with the 6-31G(d) basis set was successfully applied to describe the geometry and the vibrational structure of CO-ligated heme. In addition, it was reported recently that among the 6-311G(2d), 6-311G+(2d), TZV, and SDD (Stuttgart−Dresden pseudopotential) basis sets, the 6-311G+(2d) basis set in combination with the B3LYP functional could well describe the character of a small transition-metal complex like Fe−CO with regard to the electronic configuration with a given multiplicity, the correct order of the two lowest excited states, and their energy separation.[17] We thus employed the two sets of basis sets in order to see whether there is a basis set dependency of the obtained results. The vertical excitation energy computation employing the TD-DFT method[9] with the B3LYP functional was reported to give a balanced error for both B and Q bands of a heme−CO adduct with the overestimations of 0.2−0.3 eV.[7b]

Our DFT study is comprised of the geometry optimization of the heme−CO adducts (**1**−**3**), vibrational analyses of the fully converged structures, and the TD-DFT computations of the vertical excitation energy of the 5cH and 6cH−Im. Since, currently, it is difficult to obtain the Hessian of an excited-state molecule within the framework of the TD-DFT theory, an intrinsic reaction coordinate could not be predictable. Hence, to simulate the photochemical reaction coordinate of photodissociable 6cH−Im and photoinert 5cH, we assumed that the singlet excitation of the heme complexes results in the formation of the energetically lowest excited spin states. Therefore, the geometrical changes from the singlet state to the quintet state of the 6cH−Im and from the singlet state to the triplet state of the 5cH were traced by the Berny geometry optimization procedure as implemented in the Gaussian 98 program package: the singlet ground states of the 6cH−Im and 5cH were optimized using the geometry of the quintet 6cH−Im and the triplet 5cH, respectively, as the initial coordinates, and the reverse order of the obtained coordinates (i.e., from the singlet to the excited spin states) was assumed to be the photochemical reaction coordinates of the 6cH−Im and 5cH. The advantage of our simulated reaction coordinates is that effects of heme distortion and Fe−C−O bending on CO dissociation from the heme could be investigated, which have not been taken into consideration in the previous calculations.[7a,b]

Results and Discussion

I. Molecular Properties of the Ground-State Heme−CO Adducts. Nowadays, it is well established that the ground-state geometry of the Fe−C−O unit of a 6cH−Im is linear, while in a protein matrix, it is slightly distorted mainly because of electrostatic perturbation from the distal environment.[18,19] The linear Fe−C−O structure with a singlet spin state was also computed as the ground state for 5cH and 6cH−H_2O in this study. We did not see any significant basis set dependency in the description of the ground-state geometries of the heme−CO adducts, as shown in Table 1. In the frequency analysis, however, the C−O stretching (ν_{C-O}) frequency was significantly dependent on the basis sets, as indicated in Table 1. Judging from the ν_{C-O} frequencies, the C−O bond estimated by the 6-31G(d) (BS1) basis set seems to be much harder than the one computed by the 6-311G+(2d) (BS2) basis set for all species. Computation on the 6cH−Im as a reference molecule for comparison with the reported experimental values[20] suggests

TABLE 1: Selected Optimized Geometrical Parameters and Vibrational Frequencies of the Singlet Ground State of Heme−CO Adducts[a]

	5cH	6cH−H_2O	6cH−Im
	Geometrical Parameters (Å)		
Fe−C	1.72 (1.72)	1.76 (1.75)	1.78 (1.77)
C−O	1.17 (1.15)	1.17 (1.15)	1.17 (1.15)
Fe−N_{Por}[b]	2.01 (2.00)	2.02 (2.01)	2.02 (2.02)
Fe−L_{Axial}		2.12 (2.12)	2.08 (2.07)
Fe−<heme plane>[c]	0.20 (0.19)	0.12 (0.11)	0.03 (0.04)
C_α−C_β[b]	1.44 (1.44)	1.44 (1.44)	1.45 (1.45)
C_α−C_m[b]	1.39 (1.39)	1.39 (1.39)	1.39 (1.39)
C_β−C_β[b]	1.36 (1.36)	1.36 (1.36)	1.36 (1.36)
	Vibrational Frequencies (cm^{-1})		
Fe−C−O deformation	498(497)	537 543 (541 545)	560 566 (569 576)
Fe−CO stretch	579 (575)	526 (522)	497 (493)
C−O stretch	1935 (2089)	1943 (2097)	1940 (2099)
ν_4	1408 (1408)	1406 (1405)	1405 (1405)
ν_3	1503 (1504)	1494 (1496)	1493 (1494)
ν_2	1620 (1620)	1613 (1614)	1612 (1613)
ν_{10}	1691 (1693)	1675 (1677)	1667 (1669)

[a] The computed values were obtained by using the 6-311G+(2d) (Fe and CO) and 6-31G(d) (other atoms) basis sets (BS2) and the values in parentheses were by the 6-31G(d) basis set for all atoms (BS1). 5c has no symmetry, while 6c−H_2O and 6c−Im involve *Cs* symmetry. [b] The averaged distances. [c] The heme plane is defined by three arbitrarily selected porphyrin nitrogen atoms.

that the BS2 basis set more properly represents the Fe−C−O bonding compared to the BS1 basis set.

Within the two levels of approximation adopted, we can reasonably conclude that the Fe−C bond distances are elongated and the ν_{Fe-CO} frequencies are decreased proportionally as the axial donation ability increases. The ν_{Fe-CO} frequency (579 cm^{-1}) of the 5cH is much higher than the experimental values (520−530 cm^{-1})[21] but is also reported by Spiro and co-workers, who used DFT calculations.[19b] Indeed, the Fe−CO binding energy of 5cH was computed to be 23.8 kcal/mol, which is 14 kcal/mol larger than that of 6cH−Im. The ν_{Fe-CO} frequency of 6cH−H_2O (526 cm^{-1}) is reasonably intermediate among the three heme−CO adducts. Thus, the Fe−CO bond is much stronger in 5cH than in 6cH−Im in their ground-state electronic structures. However, this does not ensure that the Fe−CO bond in 5cH is more stable than that in 6cH−Im under photoexcited conditions, because the photoreactivity might be dependent on the excited-state potential along a reaction coordinate, and investigation into the excited state is essential to answer the question whether 5cH is photoinert or not.

It is worth noting that the Fe−C−O bending (δ_{FeCO}) frequency of 5cH is lower than the ν_{Fe-CO} frequency, which is opposite to the case of the 6c heme−CO adducts. Thus, ligation of a ligand at the trans position in the heme−CO adducts significantly alters the property of the Fe−C−O bonding. Then, a question arises as to what kind of electronic effects lead to a decrease of the Fe−C−O bending restoring force. To answer to this question, we have to introduce the vibronic interaction theory, which correlates the mixing of electronic states with nuclear displacements. Vibronic interaction theory provides a systematic approach to establish the correlation between the electronic structure, bonding geometry, and photoreactivity.[22,23] For a diatomic molecule (XO) adduct of heme with a linear geometry of Fe−X−O, there is a possibility of dipolar instability due to a pseudo-Jahn−Teller effect, which tends to distort the linear configuration along a bending normal coordinate.[22,23] To rationalize the possible strong vibronic interaction in softening the Fe−C−O bending potential in 5cH, we first examine the orbital interaction diagram of the heme−CO adducts below.

TABLE 2: Calculated Atomic Charges of FeCO[a]

atom	5cH	6cH−H_2O	6cH−Im
Fe	1.19 (0.90)	1.18 (0.89)	1.14 (0.85)
C	0.08 (0.28)	0.13 (0.33)	0.15 (0.32)
O	−0.28 (−0.30)	−0.29 (−0.22)	−0.28 (−0.30)

[a] The computed values were obtained by using the BS2 basis set and the values in parentheses were by the BS1 basis set for all atoms.

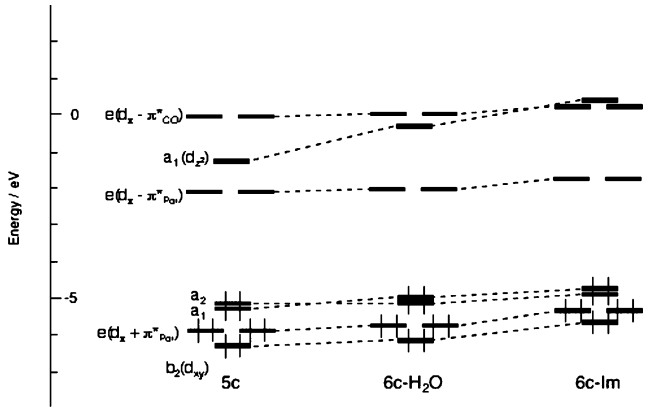

Figure 1. Orbital interaction diagram of the heme−CO adducts.

The ν_4 Raman band, a marker band for π delocalization in the macrocycle,[24] which is composed of C_α−C_β and C_α−N_{por} symmetric stretching, is almost insensitive to ligation to the trans position of CO. The ν_2 and ν_3 bands,[24] which primarily consist of C_β−C_β and C_α−C_m symmetric stretching, respectively, are sensitive to the coordination numbers but may not be useful to distinguish between coordinations of a weak ligand like water and a strong ligand like imidazole at axial positions. On the other hand, the ν_{10} band,[24] which is composed of the out-of-phase C_α−C_m symmetric stretchings, seems to be quite sensitive to electron density delocalization from the trans axial ligand, and thus, it can be an indicator of the extent of electronic coupling between the axial ligand orbitals and porphyrin C_α−C_m π* orbitals (antibonding) through the π system of the Fe and pyrrole N atoms.

Table 2 gives the atomic charges on Fe and CO. The effect of the axial ligation is clearly seen in the shift of the charge from C to Fe in both approximations. The charge shift from C to Fe is most significant in the imidazole-ligated model and less upon the change from 6cH−H_2O to 5cH. According to the Dewar, Chatt, and Duncanson (DCD) model,[25,26] the strength of M−CO bond is determined by a balance between π-back-donation from metal to the CO π* orbital (which could be correlated to the C−O bond length) and σ donation from the C lone pair to the vacant d_{z^2} orbital of Fe (which could be correlated with Fe−C distance). The latter interaction is repulsive, and thus, that the more the σ donation is, the weaker the Fe−C bond is in the computed models is compatible with the DCD view.

II. Orbital Interaction Diagrams of the Ground State of the Heme-CO Adducts. The frontier orbital diagrams of the heme−CO adducts are shown in Figure 1. Symmetry labeling of the orbitals is based on C_{4v} symmetry assumed to all the molecules. The orbital energy levels are drawn from the calculations with the BS2 basis set.

We note that the energy level of the $a_1(d_{z^2})$ (the antibonding σ* orbital composed of the d_{z^2} orbital of Fe and the p orbital of the ligands) orbital is altered significantly by the axial donation. As the axial donation becomes stronger, the $a_1(d_{z^2})$ level is elevated. Let us now consider why the Fe−C−O bending

potential is so softened in the 5cH. Within the framework of C_{4v} symmetry, the Fe−C−O distortion belongs to coordinates of the *E* species. According to the vibronic interaction theory,[22,23] the mixing of the a_1 and *e* electronic states, the direct product of which involves *E* vibration, can decrease the curvature of the adiabatic potential in the direction of the *E* displacements. The energy of the mixed states is given by eq 1 as a function of the mixing coordinate, Q_k,

$$E_{\pm} = \frac{1}{2}F_{kk}Q_k^2 \pm \Delta\left(1 + \frac{f_k^2}{\Delta^2}Q_k^2\right)^{1/2} \quad (1)$$

where F_{kk} is the harmonic force constant and f_k is the linear vibronic coupling constant

$$F_{kk} = \langle\psi_i|(\partial^2 V/\partial Q_k^2)_0|\psi_i\rangle \qquad (i \text{ is } A_1 \text{ or } E) \quad (2)$$

$$f_k = \langle\psi_i|(\partial V/\partial Q_k)_0|\psi_j\rangle \qquad [i \neq j\ (A_1, E)] \quad (3)$$

The role of the linear vibronic coupling constant is to soften the adiabatic potential along the mixing coordinate. Δ is half the a_1−*e* energy separation in the absence of mixing. After expanding the second term in *Q* of eq 1,

$$E_{\pm}(Q_k) = \frac{1}{2}\left(F_{kk} \pm \frac{f_k^2}{\Delta}\right)Q_k^2 \pm \frac{f_k^4 Q_k^4}{\Delta^3} \mp \cdots \quad (4)$$

It is seen from these expressions that the two adiabatic potential curves change in different ways as a result of the vibronic coupling: in the upper sheet, the curvature increases, whereas in the lower one, it decreases. If the mixing is strong enough with small Δ and large f_k ($\Delta < f_k^2/F_{kk}$), the coefficient of the second-order term of *Q* in eq 4 for the lower adiabatic potential curve becomes negative and its combination with the positive biquadratic term results in a double minimum potential. Thus, the molecule distorts along the mixing coordinate. If $f_k^2/F_{kk} < \Delta$, this is the case of a weak pseudo-Jahn−Teller effect, in which the minima of both states remain at the point $Q = 0$ but the adiabatic potential along the mixing coordinate becomes soft. Thus, the efficiency of the a_1 and *e* mixing is critically dependent on the energy gap (Δ) between the $a_1(d_{z^2})$ and $e(d_\pi + \pi_{por}^*)$ orbitals in the case of the singlet ground state. Indeed, the Fe−C−O bending potentials were computed to be softer as the unoccupied $a_1(d_{z^2})$ level becomes lower.

While the energy gap between the unoccupied $a_1(d_{z^2})$ and occupied $e(d_\pi + \pi_{por}^*)$ orbitals is still large in 5cH, once the nearly degenerate LUMO of the $e(d_\pi - \pi_{por}^*)$ orbital is occupied by electron density upon light irradiation, it might be expected that the strong mixing between the $a_1(d_{z^2})$ and the $e(d_\pi - \pi_{por}^*)$ orbitals causes dipolar instability, which results in a bent Fe−C−O conformation.

III. Geometries, Vibrations, and Energetics of the High (Quintet) and Intermediate (Triplet) Spin States of the Heme−CO Adducts. We extensively investigated the quintet and triplet spin states of the heme−CO adducts, because the intersystem crossing from the ground singlet spin state to the excited multiple spin states might be one of the key processes in the photochemistry of heme−CO complexes.[3,4] First, we examined the properties of the excited spin states of 5cH. The optimized molecular structures are delineated in Figure 2, while the selected optimized geometries and the selected vibrational modes and frequencies are given in Table 3. The triplet state was computed as the ground state of the excited spin states of 5cH, and the triplet state and the quintet state are 8.0 and 10.3 kcal/mol, respectively, higher in energy than the singlet.

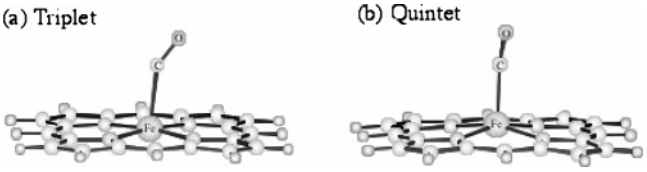

Figure 2. Structure of 5cH in the (a) triplet and (b) quintet spin states.

TABLE 3: Selected Geometrical Parameters and Relative Energies of the Excited Spin States of 5c CO−Heme Adduct[a]

	triplet	quintet
Bond Distances (Å)		
Fe−C	2.20	2.07
C−O	1.15	1.15
Fe−N_{Por}[b]	2.01	2.08
Fe−<heme plane>[c]	0.12	0.20
C_α−C_β[b]	1.44	1.45
C_α−C_m[b]	1.39	1.40
C_β−C_β[b]	1.36	1.37
Bond Angles (deg)		
Fe−C−O bend	147.9	170.3
Fe−C tilt	5.9	2.4
Vibrational Frequencies (cm^{-1})[d]		
Fe−C−O bending	209	255
Fe−C−O wagging	159	283
Fe−CO stretch	155	267
C−O stretch	1974	1988
ν_4	1407	1395
ν_3	1496	1474
ν_2	1614	1596
ν_{10}	1679	1648

[a] The computed values are obtained using the BS2 basis set, and no symmetry was imposed on the molecules. [b] The averaged values. [c] The heme plane is defined by three arbitrarily selected nitrogen atoms. [d] No imaginary vibrational frequency was computed for both spin state species.

As might be expected, the geometry of Fe−C−O is distorted in both excited spin states. The triplet species involves more bent Fe−C−O and less out-of-plane displacement of iron compared to those of the quintet species. The Fe−CO bond is more lengthened in the triplet state than in the quintet state, and thus, the Fe−C−O deformation is effective in activation of the Fe−CO bond. The mechanism of the Fe−C−O distortion and iron out-of-plane displacement in the excited spin states would be rationalized on the basis of the vibronic interaction theory.[22,23] Within the framework of C_{4v} symmetry, the Fe−C−O distortion and the iron out-of-plane displacement are contained in the *e* and a_1 excited states, respectively. As pointed out in Figure 1, electron densities in the excited spin states would be placed on the $e(d_\pi - \pi_{por}^*)$ orbitals (LUMO), and the partially occupied $e(d_\pi - \pi_{por}^*)$ orbitals would begin to interact with the upper unoccupied orbitals. The orbital mixing between the $e(d_\pi - \pi_{por}^*)$ and $a_1(d_{z^2})$ orbitals [$E \times A_1 = E$] would stabilize the Fe−C−O distortion, and the mixing between the $e(d_\pi - \pi_{por}^*)$ and $e(d_\pi - \pi_{CO}^*)$ orbitals [$E \times E = A_1 + A_2 + B_1 + B_2$] would enhance the out-of-plane distortion (A_1 species). The frequencies of the Fe−CO stretching and Fe−C−O distortion vibrations in both spin states are lowered significantly compared with those of the singlet ground state with linear geometry. Since the quintet state involves a more distorted heme compared with that of the triplet state, the vibrational frequencies of the porphyrin maker bands in the quintet state are decreased.

6cH−H_2O was also computed, and it was found that 6cH−H_2O forms a stable Fe−CO bond in the excited spin states, as

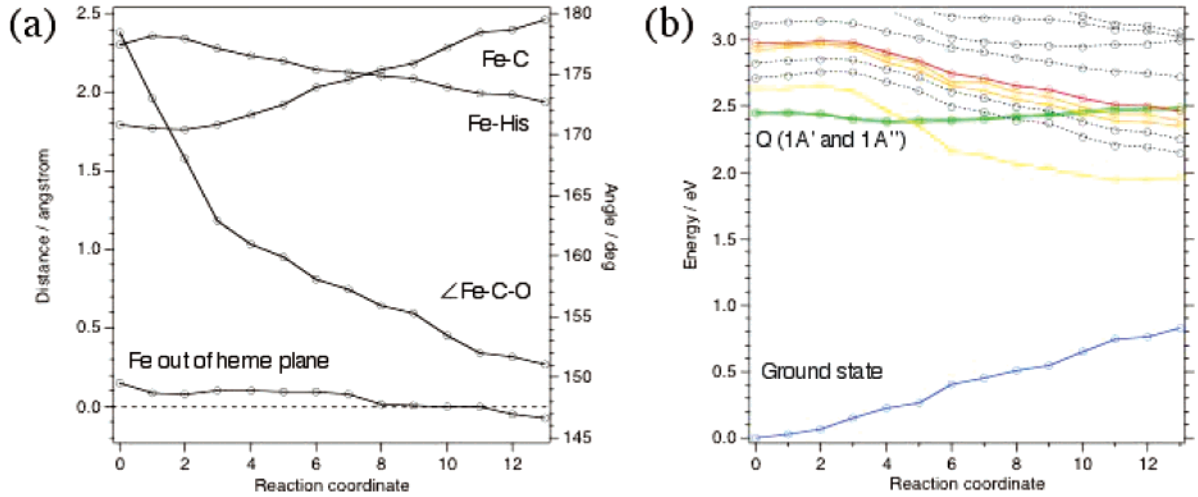

Figure 3. (a) Selected geometrical parameter changes of 6cH−Im along the simulated photoexcited reaction coordinate. (b) Potential energy curves of the ground state and singlet excited states of 6cH−Im along the reaction coordinate described in part a computed by TD-DFT/B3LYP/BS2 theory level. The blue line is the potential energy curve of the ground state, and the green, yellow, orange, and red lines correspond to the Q, 2A′, 4A′ and 4A″, and 5A′ states, as listed in Table 4, respectively.

shown in Figure S1 and Tables S1 and S2 in the Supporting Information. The ground state geometries of both excited spin states are nearly linear Fe−C−O, but the bent forms were also fully converged in the geometry optimizations, which were higher by only 0.6−1 kcal/mol from the linear form, as shown in Figure S2 and Table S3 and S4 in the Supporting Information. Interestingly, the axial water ligand is dissociated in the Fe−C−O distorted forms. Thus, the stable Fe−CO bonding is considered to be achieved on account of the weaker affinity of the water ligand to the ferrous iron compared with that of CO, and thereby, the iron out-of-plane displacement due to the vibronic interaction is directed to CO.

On the other hand, the imidazole-bound 6c CO-bound heme was reported to form the Fe···CO nonbonding van der Waals complexes as the ground state of high spin states.[27,28] In other words, the Fe−CO bond is unstable in the excited spin state. The formation of the Fe−CO bond in the excited spin states might be responsible for the presence of the apparently nonphotodissociable CO-ligated heme. It is highly likely that the CO molecule ligated to the heme with a weak trans ligand is also not photodissociable. In fact, Spiro and co-workers reported that CO-ligated PEG-modified HRP in benzene, in which the axial His ligation was weakened, was stable against intense laser irradiation.[29]

IV. Characterization of the Excited States of the Photodissociable 6cH−Im and the Nonphotodissociable 5cH. We will discuss here why 5cH was hardly photodissociable compared with 6cH−Im on the basis of the excited-state profiles obtained by the TD-DFT calculation along simulated reaction coordinates. The reaction coordinate of 6cH−Im is shown in Figure 3a.

The dissociation of CO from 6cH−Im is initiated by the Fe−C−O bending, and the Fe−CO bond is not elongated until the Fe−C−O angle becomes 165°. This CO dissociation mechanism including Fe−C−O bending would be related to an observation by Anfinrud and co-workers that a photolyzed CO dipole became parallel to the heme plane within ∼0.5 ps of the CO photolysis.[30] Such a rapid change in the ligand orientation would be facilitated if CO dissociation occurs along the Fe−C−O bending coordinate as shown in Figure 3a. The positive out-of-plane displacement means that the Fe of the 6cH−Im moves toward the CO ligand with an indicated distance, while the negative value means that the Fe is displaced toward the imidazole ligand. Thus, the simulated coordinate for CO photolysis from 6cH−Im also includes the out-of-plane displacement of Fe, which was not taken into consideration in the previous calculations,[7a,b] and would have relevance to an experimental observation that the out-of-plane motion of Fe takes place within 300 fs after the photoexcitation. The heme-bound CO is dissociated at reaction coordinate #10, because, at this stage, the Fe−CO is elongated to 2.3 Å and the Fe is placed out of the heme plane toward the imidazole ligand.

TABLE 4: Selected Excited States of 6cH−Im

state	configuration	property	*E*/eV
1A′ (Q)	115 → 122 (−0.23)	$e(d_\pi + \pi_{CO}^*) \rightarrow a_1(d_{z^2})$	2.4428
	117 → 119 (0.45)	$a_1 \rightarrow e(d_\pi - \pi_{por}^*)$	
	118 → 120 (0.47)	$a_2 \rightarrow e(d_\pi - \pi_{por}^*)$	
1A″ (Q)	116 → 122 (−0.13)	$e(d_\pi + \pi^*_{CO}) \rightarrow a_1(d_{z2})$	2.4521
	117 → 119 (−0.46)	$a_1 \rightarrow e(d_\pi - \pi_{por}^*)$	
	118 → 120 (0.51)	$a_2 \rightarrow e(d_\pi - \pi_{por}^*)$	
2A′	114 → 122 (0.40)	$b_2(d_{xy}) \rightarrow a_1(d_{z^2})$	2.6339
	114 → 124 (0.12)	$b_2(d_{xy}) \rightarrow e(d_\pi - \pi_{CO}^*)$	
	115 → 119 (−0.41)	$e(d_\pi + \pi_{CO}^*) \rightarrow e(d_\pi - \pi_{por}^*)$	
	115 → 123 (−0.10)	$e(d_\pi + \pi_{CO}^*) \rightarrow e(d_\pi - \pi_{CO}^*)$	
	116 → 120 (−0.34)	$e(d_\pi + \pi_{CO}^*) \rightarrow e(d_\pi - \pi_{por}^*)$	
4A′	114 → 119 (0.67)	$b_2(d_{xy}) \rightarrow e(d_\pi - \pi_{por}^*)$	2.9219
	114 → 123 (0.11)	$b_2(d_{xy}) \rightarrow e(d_\pi - \pi_{CO}^*)$	
	115 → 126 (−0.16)	$e(d_\pi + \pi_{CO}^*) \rightarrow b_1(d_{x^2-y^2})$	
4A″	114 → 120 (0.67)	$b_2(d_{xy}) \rightarrow e(d_\pi - \pi_{por}^*)$	2.9526
	114 → 124 (0.10)	$b_2(d_{xy}) \rightarrow e(d_\pi - \pi_{CO}^*)$	
	116 → 126 (0.17)	$e(d_\pi + \pi_{CO}^*) \rightarrow b_1(d_{x^2-y^2})$	
5A′	114 → 122 (0.41)	$b_2(d_{xy}) \rightarrow a_1(d_{z^2})$	2.9820
	114 → 124 (0.13)	$b_2(d_{xy}) \rightarrow e(d_\pi - \pi_{CO}^*)$	
	115 → 119 (0.32)	$e(d_\pi + \pi_{CO}^*) \rightarrow e(d_\pi - \pi_{por}^*)$	
	116 → 120 (0.33)	$e(d_\pi + \pi_{CO}^*) \rightarrow e(d_\pi - \pi_{por}^*)$	

In Figure 3b, the obtained excited-state profile of 6cH−Im against various coordinates is depicted, providing much insight into the photodissociation process of 6cH−Im.[7a,b] It is postulated in this calculation that the system at the ground state is excited into the Q state by a laser pulse of 2.4 eV. According to our calculations, the Q (1A′ and 1A″) state involves a minor Fe−CO repulsive state, as listed in Table 4. The Q state, shown by green lines in Figure 3b, starts crossing one of the Fe−CO repulsive states, 2A′ (yellow line), at reaction coordinate #4. Up to this stage, the reaction proceeds along the Fe−C−O bending coordinate until 160°. It would, thus, be suggested for photoexcitation to the Q state that the vibrational wave packet on the excited state profile has intrinsically dissociative character

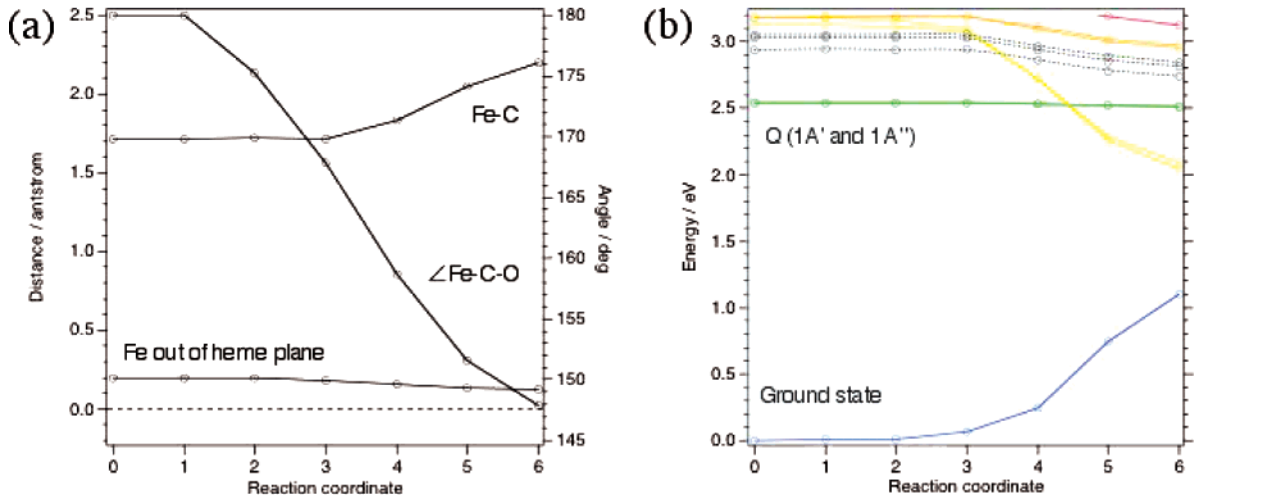

Figure 4. (a) Selected geometrical parameter changes of 5cH along the simulated photoexcited reaction coordinate. (b) Potential energy curves of the ground state and singlet excited states of 5cH along the reaction coordinate described in part a computed by TD-DFT/B3LYP/BS2 theory level. The blue line is the potential energy curve of the ground state, and the green, yellow, orange, and red lines correspond to the Q, 4A′ and 5A″, 6A′ and 6A″, and 7A′ states, as listed in Table 5, respectively.

TABLE 5: Selected Excited States of 5cH

state	configuration	property	*E*/eV
1A′ (Q)	99 → 101 (0.49)	$a_1 \rightarrow e(d_\pi - \pi_{por}^*)$	2.5452
	100 → 102 (0.52)	$a_2 \rightarrow e(d_\pi - \pi_{por}^*)$	
1A″ (Q)	99 → 102 (−0.49)	$a_1 \rightarrow e(d_\pi - \pi_{por}^*)$	2.5454
	100 → 101 (0.52)	$a_2 \rightarrow e(d_\pi - \pi_{por}^*)$	
4A′	97 → 102 (0.37)	$e(d_\pi + \pi_{CO}^*) \rightarrow e(d_\pi - \pi_{por}^*)$	3.1276
	98 → 101 (−0.34)	$e(d_\pi + \pi_{CO}^*) \rightarrow e(d_\pi - \pi_{por}^*)$	
	99 → 103 (0.46)	$a_1 \rightarrow a_1(d_{z^2})$	
5A″	100 → 103 (0.70)	$a_2 \rightarrow a_1(d_{z^2})$	3.1821
6A′	96 → 101 (0.65)	$b_2(d_{xy}) \rightarrow e(d_\pi - \pi_{por}^*)$	3.1842
	96 → 106 (0.16)	$b_2(d_{xy}) \rightarrow e(d_\pi - \pi_{CO}^*)$	
	97 → 107 (−0.18)	$e(d_\pi + \pi_{CO}^*) \rightarrow b_1(d_{x^2-y^2})$	
6A″	96 → 102 (0.66)	$b_2(d_{xy}) \rightarrow e(d_\pi - \pi_{por}^*)$	3.1855
	96 → 105 (−0.11)	$b_2(d_{xy}) \rightarrow e(d_\pi - \pi_{CO}^*)$	
	98 → 107 (−0.19)	$e(d_\pi + \pi_{CO}^*) \rightarrow b_1(d_{x^2-y^2})$	
7A′	97 → 102 (−0.30)	$e(d_\pi + \pi_{CO}^*) \rightarrow e(d_\pi - \pi_{por}^*)$	3.4831
	98 → 101 (−0.30)	$e(d_\pi + \pi_{CO}^*) \rightarrow e(d_\pi - \pi_{por}^*)$	
	99 → 103 (0.49)	$a_1 \rightarrow a_1(d_{z^2})$	

on the Fe−CO bond, which can be further induced by the bending motion. At reaction coordinate #10, where the CO dissociation is considered to take place, the Q state crosses Fe to porphyrin CT states (4A′ and 4A″, orange lines) and an Fe−CO σ^* (5A″, red line) repulsive state. Therefore, such a decay of the Q state would be the essential character for the CO photolysis. The barrier that must be overcome for this decay is about 0.05 eV, which is significantly lower than the 0.2 eV computed for the linear Fe−CO stretching dissociation coordinate.[7a,b] Therefore, the Fe−C−O bending is effective to derive the Fe−CO dissociative state, as previously proposed by Waleh and Loew.[31] The Fe−C−O bending and Fe−CO stretching frequencies of 6cH−Im are 560−566 cm^{-1} and 497 cm^{-1}, respectively, corresponding to a 60−70 fs time regime, which correlates well with the observed time scale of the photodissociation process of 50 fs. Thus, the dissociation of CO occurs within one vibrational period of those displacements.

Next, the reaction coordinate and the excited state profile of the hardly photodissociable 5cH are shown in Figure 4a and b, respectively. While the reaction coordinate of 5cH seems to be similar to that of 6cH−Im, the property of the excited state exhibits different features from those of the photodissociable 6cH−Im. The Q state of 5cH is the pure $\pi-\pi^*$ transition of porphyrin, as listed in Table 5. The reaction is led by the Fe−C−O bending up to 160°, and the Q state (green lines) crosses the two Fe−CO repulsive states, 4A′ and 5A′ (yellow lines in Figure 4b), at reaction coordinate #4. Interestingly, even at reaction coordinate #6, where the Fe···CO separation is 2.2 Å, the Fe to porphyrin CT state (6A′ and 6A″, orange lines) and the Fe−CO σ^* state (7A″, red line) do not cross the Q state (1A′ and 1A″). The barriers against populating in both the Fe−CO dissociative and the Fe-to-porphyrin CT states are 0.6 eV, which is much higher than that of 6cH−Im. Thus, cleavage of the Fe−CO bond in the final reaction product requires 0.6 eV of extra energy, which would be an unfavorable reaction because formation of the triplet state with stable Fe−CO bonding has an energy cost of 0.3 eV, which is half of the barrier for the CO photolysis. This large barrier and the slow decay of the Q state into the Fe−CO repulsive as well as Fe-to-porphyrin CT states in 5cH would be deeply concerned with the mechanism of the photoinert heme−CO adduct. Hence, the photoisomerization from the linear to bent Fe−C−O seems to be indispensable to make a 5c heme−CO adduct photoinert.

Even though the Fe−CO bond could be cleaved thermally, the CO rebinding rate would be very fast because this binding does not require the spin state change of the heme. In fact, a proximal ligation effect on the kinetics of CO binding was examined by Champion et al. recently, demonstrating that absence of the axial ligation increased the CO rebinding rate 45 times faster than in the case of its presence.[32] Studies by Dlott et al.[33] and Friedman et al.[34] demonstrated picosecond geminate recombination for CO under conditions where the proximal histidine−iron bond is ruptured. On the other hand, a strong hydrogen-bonding network to heme-bound CO from a distal environment was proposed to prevent a CO-bound truncated Hb O (trHbO−CO) from efficient CO photolysis, and picosecond geminate CO rebinding was also suggested, which was ascribed to the peculiar distal environment.[35] The effect of a hydrogen bond to heme-bound CO is known to cause back-bonding from the heme to the CO π^* orbital that results in weakening of the C−O bond and concomitant strengthening of the Fe−CO bond.[19b] As we looked at the orbital interaction diagram in Figure 1, the strengthening of the Fe−CO bond would result in the lowering of the $a_1(d_{z^2})$ orbital level with dominance of the CO σ orbital contribution in competition with the σ orbital of the trans axial ligand for the Fe d_{z^2} orbital. Thus, the strength of the hydrogen bond can alter the $a_1(d_{z^2})$ orbital level indirectly, which in turn wouldaffect Fe−CO bonding

stability in excited states. To understand the CO rebinding kinetics under the influence of a protein matrix, a molecular dynamics simulation is required, and that is of our future interest.

Conclusion

To understand the mechanism by which the 5c heme−CO adduct becomes apparently nonphotodissociable, we have carried out hybrid DFT calculations on the geometrical and vibrational aspects of the singlet and excited spin states of the 5c heme−CO adduct, and some of these properties were compared with those of the water-ligated 6c heme−CO adduct and the imidazole-ligated 6c heme−CO adduct. The results indicated that the 5c heme−CO adduct and the 6c heme−CO adduct, which has weak trans ligation, could retain Fe−CO bonding with a distorted Fe−C−O conformation in the excited spin states. It was found that when the axial ligation at the trans of CO is absent or weak, the out-of-plane displacement of Fe induced by the vibronic interaction is directed toward the CO ligand, thereby allowing the Fe−CO bond to be stable in the excited spin states. On the contrary, the imidazole-ligated 6c heme−CO adduct has been known to have dissociative Fe−CO bonding in the excited spin states, in which the Fe out-of-plane displacement is directed toward the imidazole ligand.

The TD-DFT computations revealed that the Q state of 6cH−Im involves a minor Fe−CO dissociative state. The Fe−C−O bending, which can be enhanced through a pseudo-Jahn−Teller mechanism, has been shown to lead to an Fe−CO dissociative state in the excited-state potential without elongation of the Fe−CO bond. When the Fe···CO separation is 2.3 Å, the Q state decays into Fe−CO repulsive states as well as Fe-to-porphyrin CT states with a barrier of 0.05 eV, resulting in the dissociation of CO. On the other hand, the Q state of 5cH neither includes the Fe−CO dissociative character nor crosses the corresponding Fe−CO dissociative state or Fe-to-porphyrin CT state even at an Fe···CO distance of 2.2 Å. The barrier that must be surmounted to lead to the Fe−CO repulsive states in 5cH at the final reaction coordinate was calculated to be 0.6 eV, which would be an unfavorable reaction compared with formation of the triplet state with the stable bent Fe−C−O bond.

Thus, we are led to propose that possible photoisomerization from the ground-state linear to the bent Fe−C−O in 5cH would prevent CO from photolysis. The nonphotodissociable heme−CO adduct may effectively convert the excitation photon energy into the distortion energy of heme, which may later be used to excite the Fe−C−O bending vibration and to induce the iron out-of-plane displacement. While such an Fe−C−O distorted excited species of a heme−CO adduct has never been identified spectroscopically, it is very desirable that the bent heme−CO adduct is detected by an ultrafast technique to clarify the photophysical chemistry of heme in the future. It is of future interest, by using excited-state dynamic theory,[36] to understand how energy stored by the illumination of a heme−CO adduct flows inside of the chromophore and to which reaction channels the CO photolysis opens between Fe−CO stretching and Fe−C−O bending coordinates.

Acknowledgment. We thank Prof. P. M. Kozlowski (University of Louisville), who has visited Okazaki through JSPS Invitation Fellowship Programs for Research in Japan, for helpful comments and discussion. This study was supported by a JSPS Fellowship to T.O. and B.P. and by a Grant-in-Aid for Specifically Promoted Research to T.K. (14001004) from the Ministry of Education, Culture, Sports, Science, and Technology, Japan. The computations were partly carried out with a help from the Research Center for Computational Science at the Okazaki Research Facilities, National Institutes of Natural Sciences.

Supporting Information Available: Figures S1 and S2 and Tables S1−S4. This material is available free of charge via the Internet at http://pubs.acs.org.

References and Notes

(1) Bucher, T.; Kaspers, J. *Biochim. Biophys. Acta* **1947**, *1*, 21−34.

(2) (a) Schuresko, D. D.; Webb, W. W. *Biophys. J.* **1978**, *24*, 382−383. (b) Ye, X.; Demidov, A.; Champion, P. M. *J. Am. Chem. Soc.* **2002**, *124*, 5914−5924.

(3) Franzen, S.; Kiger, L.; Poyart, C.; Martin, J. L. *Biophys. J.* **2001**, *80*, 2372−2385.

(4) Petrich, J. W.; Poyart, C.; Martin, J. L. *Biochemistry* **1988**, *27*, 4049−4060.

(5) Greene, B. I.; Hochstrasser, R. M.; Weisman, R. B.; Eaton, W. A. *Proc. Natl. Acad. Sci. U.S.A.* **1978**, *75*, 5255−5259.

(6) Mizutani, Y.; Kitagawa, T. *J. Phys. Chem. B* **2001**, *105*, 10992−10999.

(7) (a) Dreuw, A.; Dunietz, B. D.; Head-Gordon, M. *J. Am. Chem. Soc.* **2002**, *124*, 12070−12071. (b) Dunietz, B. D.; Dreuw, A.; Head-Gordon, M. *J. Phys. Chem. B* **2003**, *107*, 5623−5629. (c) Angelis, F. D.; Car, R.; Spiro, T. G. *J. Am. Chem. Soc.* **2003**, *125*, 15710−15711.

(8) (a) Pal, B.; Li, Z.; Ohta, T.; Takenaka, S.; Tsuyama, S.; Kitagawa, T. *J. Inorg. Biochem.* **2004**, *98*, 824−832. (b) Pal, B.; Ohta, T.; Kitagawa, T. unpublished results. (c) Ohta, T.; Pinakoulaki, E.; Soulimane, T.; Kitagawa, T.; Varotsis, C. *J. Phys. Chem. B* **2004**, *108*, 5389−5491.

(9) Casida, M. E. In *Recent Advances in Density Functional Methods, Part I*; Chon, D. P., Ed.; World Scientific: Singapore, 1995.

(10) Frisch, M. J.; Trucks, G. W.; Schlegel, H. B.; Scuseria, G. E.; Robb, M. A.; Cheeseman, J. R.; Zakrzewski, V. G.; Montgomery, J. A.; Stratmann, R. E.; Burant, J. C.; Dapprich, S.; Millam, J. M.; Daniels, A. D.; Kudin, K. N.; Strain, M. C.; Farkas, O.; Tomasi, J.; Barone, V.; Cossi, M.; Cammi, R.; Mennucci, B.; Pomelli, C.; Adamo, C.; Clifford, S.; Ochterski, J.; Petersson, G. A.; Ayala, P. Y.; Cui, Q.; Morokuma, K.; Malick, D. K.; Rabuck, A. D.; Raghavachari, K.; Foresman, J. B.; Cioslowski, J.; Ortiz, J. V.; Stefanov, B. B.; Liu, G.; Liashenko, A.; Piskorz, P.; Komaromi, I.; Gomperts, R.; Martin, R. L.; Fox, D. J.; Keith, T.; Al-Laham, M. A.; Peng, C. Y.; Nanayakkara, A.; Gonzalez, C.; Challacombe, M.; Gill, P. M. W.; Johnson, B. G.; Chen, W.; Wong, M. W.; Andres, J. L.; Head-Gordon, M.; Replogle, E. S.; Pople, J. A. *Gaussian 98*; Gaussian Inc.: Pittsburgh, PA, 1998.

(11) Becke, A. D. *Phys. Rev. A* **1988**, *38*, 3098−3100.

(12) Becke, A. D. *J. Chem. Phys.* **1993**, *98*, 5648−5652.

(13) Lee, C.; Yang, W.; Parr, R. G. *Phys. Rev. B* **1988**, *37*, 785−789.

(14) Krishnan, R.; Binkley, J. S.; Seeger, R.; Pople, J. A. *J. Chem. Phys.* **1980**, *72*, 650−654.

(15) Clark, T.; Chandrasekhar, J.; Spitznagel, G. W.; Schleyer, P. V. *J. Comput. Chem.* **1983**, *4*, 294−301.

(16) Frisch, M. J.; Pople, J. A.; Binkley, J. S. *J. Chem. Phys.* **1984**, *80*, 3265−3269.

(17) Pilme, J.; Silvi, B.; Alikhani, M. E. *J. Phys. Chem. A* **2003**, *107*, 4506−4514.

(18) Spiro, T. G.; Kozlowski, P. M. *Acc. Chem. Res.* **2001**, *34*, 137−144.

(19) (a) Kozlowski, P. M.; Vogel, K. M.; Zgierski, M. Z.; Spiro, T. G. *J. Porphyrins Phthalocyanines* **2001**, *5*, 312−322. (b) Vogel, K. M.; Kozlowski, P. M.; Zgierski, M. Z.; Spiro, T. G. *J. Am. Chem. Soc.* **1999**, *121*, 9915−9921.

(20) Ray, G. B.; Li, X. Y.; Ibers, J. A.; Sessler, J. L.; Spiro, T. G. *J. Am. Chem. Soc.* **1994**, *116*, 162−176.

(21) Yu, N.-T.; Kerr, E. A. *Biological Application of Raman Spectroscopy*; Spiro, T. G., Ed; John Wiley & Son, Inc.: New York; Vol. 3, pp 39−95.

(22) Bersuker, I. B.; Stavrov, S. S. *Coord. Chem. Rev.* **1988**, *88*, 1−68.

(23) Bersuka, I. B. *Electronic Structure and Properties of Transition Metal Compounds*; Wiley-Interscience: New York, 1996.

(24) Spiro, T. G.; Li, X.-Y. *Biological Application of Raman Spectroscopy*; Spiro, T. G., Ed; John Wiley & Son, Inc.: New York; Vol. 3, pp 1−37.

(25) Dewar, M. J. S. *Bull. Soc. Chim. Fr.* **1951**, *18*, C71.

(26) Chatt, J.; Duncanson, L. A. *J. Chem. Soc.* **1953**, 2939.

(27) Harvey, J. N. *J. Am. Chem. Soc.* **2000**, *122*, 12401−12402.

(28) Franzen, S. *J. Phys. Chem. B* **2002**, *106*, 4533−4542.

(29) Mabrouk, P. A.; Spiro, T. G. *J. Am. Chem. Soc.* **1999**, *120*, 10303−10309.

(30) Lim, M.; Jackson, T. A.; Anfinrud, P. A. *Science* **1995**, *269*, 962−966.

(31) Waleh, A.; Loew, G. H. *J. Am. Chem. Soc.* **1982**, *104*, 2346−2351.

(32) Cao, W.; Ye, X.; Sjodin, T.; Christian, J. F.; Demidov, A. A.; Berezhna, S.; Wang, W.; Barrick, D.; Sage, J. T.; Champion, P. M. *Biochemistry* **2004**, *43*, 11109−11117.

(33) Postlewaite, J. C.; Miers, J. B.; Dlott, D. D. *J. Am. Chem. Soc.* **1989**, *111*, 1248−1255.

(34) Iben, I. E.; Cowen, B. R.; Sanches, R.; Friedman, J. M. *Biophys. J.* **1991**, *59*, 908−919.

(35) Ouellet, H.; Juszczak, L.; Dantsker, D.; Samuni, U.; Ouellet, Y. H.; Savard, P-.Y.; Wittenberg, J. B.; Wittenberg, B. A.; Friedman, J. M.; Guertin, M. *Biochemistry* **2003**, *42*, 5764−5774.

(36) Furche, F.; Ahlrichs, R. *J. Chem. Phys.* **2002**, *117*, 7433−7447.